Deformation Behavior and Degradation on Rutherford Cabling of Nb$_3$Sn Wires

Simon C. Hopkins ⬤, Bentejui Medina-Clavijo ⬤, Cristin Rastoll ⬤, Davide Rodia ⬤, Marina Malabaila,
Christian Barth ⬤, Jerome Fleiter ⬤, Thierry Boutboul ⬤, and Amalia Ballarino ⬤

Abstract—In the production of Rutherford cables, Nb$_3$Sn strands are subjected to severe deformation; and to evaluate this degradation prior to cabling, uniaxial rolling with a thickness reduction of ∼15% has often been used. The effects of this deformation on superconducting performance differ significantly between wire designs. In this article, wire deformation behavior is investigated by image analysis of electron micrographs, and the resulting degradation of critical current and residual resistance ratio is quantified, for several designs of internal tin (RRP and distributed tin) and powder-in-tube wire in use or under study at CERN for the HL-LHC upgrade and High Field Magnets program. The suitability of uniaxial rolling as a predictor of cabling degradation is assessed and recommendations are made for improved testing procedures.

Index Terms—Critical current density, deformation, image analysis, niobium-tin, scanning electron microscopy, superconducting cables, superconducting wires.

I. INTRODUCTION

FOR the production of accelerator magnets, Nb$_3$Sn wires are assembled in the form of Rutherford cables, a transposed strand configuration in which the wire is subjected to significant mechanical deformation, especially at the edges [1], [2], [3].

In the qualification and acceptance testing of wire, uniaxial rolling is often used as a proxy for cabling deformation; but this is only a reasonable representation of the geometry far from the cable edges and for low keystone angles. The geometry of deformed strand cross-sections, the resulting degradation of critical current (I_c) and residual resistance ratio (RRR), and their dependence on cabling and rolling parameters, has been extensively studied [1], [2], [3], [4], [5], [6], [7], [8], [9], [10].

Most studies of high non-copper critical current density (J_c) Nb$_3$Sn wires concern Restacked Rod Process (RRP) wire produced by Bruker OST and powder-in-tube (PIT) wire pro-

duced by Bruker EAS [1], [2], [3], [4], [5], [6], [7], [8], [9], [10]. RRP designs are described as '*A/B*' restacks, e.g., 108/127, where *B* represents the number of positions in an hexagonal array and *A* is the number of those positions occupied by a superconducting sub-element (the remainder being copper). PIT designs are identified by the number of filaments (e.g., 192). In recent years, many such studies have taken place in the context of the High Luminosity upgrade of CERN's Large Hadron Collider (HL-LHC) and related development in the US LHC Accelerator Research Program (LARP) [11], and therefore concerned wire diameters of 0.7–0.85 mm and a subset of the available wire layouts.

Early work from Turrioni et al. [2], [4] identified the key features of the deformation of RRP and PIT wires on rolling and cabling, establishing a classification of defects, identifying the effect of sub-element spacing (Cu channel thickness), and analyzing the corresponding degradation of I_c and RRR. Polyanskii et al.'s thorough study directly correlated defects identified by microscopy with their impact on superconducting performance by magneto-optical imaging [5]. Barzi et al. then established a finite element model of strand rolling deformation [6], and identified a critical strain parameter in the Cu for the onset of sub-element merging and breakage. For the 127-stack RRP wires studied, the onset of sub-element damage was experimentally at 22% rolling reduction [7]. A comparison of 108/127 and 150/169 RRP designs at 0.7 mm and 1.0 mm found broadly similar behavior, and negligible I_c degradation for deformations up to 25% rolling reduction [8].

Brown et al. later analyzed the distribution of sub-element/filament aspect ratios, diffusion barrier breakages and the effect on RRR as a function of rolling reduction in 0.78 mm diameter wires of both RRP 108/127 and PIT 192 designs [8].

For RRP 61-stack strands extracted from cables, Turrioni et al. had earlier assessed the deformation of strands as a function of their position in the cable [2]. A recent analysis of the cross-sections of MQXF cables produced in the US HL-LHC Accelerator Upgrade Project (AUP) using RRP 108/127 wire at 0.85 mm quantified the variation in sub-element aspect ratio distributions at positions close to the cable edge, and further identified a dependence on the local orientation of the sub-element pack relative to the deformation direction [9], [10]. This study did not, however, directly explore the effect of this deformation on I_c.

Recent developments at CERN have motivated the consideration of a broader range of wire designs. A heat treatment cycle

Fig. 1. Schematic representation of the RRP wire designs.

TABLE I
CHARACTERISTICS OF THE BRUKER RRP WIRES

Property	HL-LHC		HFM			
	11 T	MQXF	ERMC-1	DEM-1.1	ERMC-0.7	DEM-0.7
Diameter (mm)	0.7	0.85	1.0	1.1	0.7	
Layout	108/127		162/169		78/91	60/91
Cu/non-Cu [a]	1.15 ± 0.1	1.2 ± 0.1	0.9 ± 0.2	0.9 ± 0.2	1.2 ± 0.2	1.6 ± 0.2
Nb:Sn	3.6 (reduced Sn)		3.4 (standard Sn)		3.6 (reduced Sn)	
Mean J_c, 4.3 K 12 T (A/mm²) [b]	2612	2722	2899	2892	2784	2795
Mean RRR	296	347	289	280	329	489
Heat treatment [c]	650 °C 50 h	665 °C 50 h	650 °C 50 h	665 °C 50 h	665 °C 50 h	665 °C 50 h

[a] Range of Cu/non-Cu permitted by specification
[b] Non-Cu J_c of (series) wire after the specified heat treatment, measured in an applied magnetic field of 12 T (reported without self-field correction)
[c] Final plateau of the manufacturer's recommended heat treatment cycle; RRP® heat treatments begin with plateaus of 48 h at 210 °C and 48 h at 400 °C

TABLE II
CHARACTERISTICS OF COMMON BARRIER WIRES: POWDER-IN-TUBE (PIT)
BUNDLE-BARRIER AND DISTRIBUTED TIN (DT)

Property	PIT-BB	DT	
	BRUKER EAS	KAT	JASTEC
Diameter (mm)	0.85	1.0	1.1
Filaments or modules (Nb + Sn)	192	138+54	138+72
Cu/non-Cu	1.2 ± 0.1	1.0 ± 0.1	1.0 ± 0.1
Mean RRR	184	295	[a]
Heat treatment	415 °C 40 h, 620 °C 120 h, 645 °C 200 h	650 °C 200 h [a]	650 °C 200 h [b]

[a] Sufficient data not available
[b] Final plateau of the manufacturer's recommended heat treatment cycle

achieving high I_c in PIT 192 wire typically results in relatively low RRR [8], [12] and high RRR degradation on rolling, which prompted the development of a 'bundle-barrier' variant in the context of the HL-LHC project. CERN's High Field Magnet (HFM) program has also required investigation of additional internal tin wire designs [13], [14], [15]. Some magnet development activities, including the FalconD [16] and R2D2 [17] collaborations with INFN (Italy) and CEA (France) respectively, have favored larger 1.0–1.1 mm diameter wires and/or graded designs requiring both a high field (1.1 mm diameter strands) and a low field (0.7 mm diameter strands) conductor [15]. New designs of Nb₃Sn wire are under development in collaboration with wire manufacturers, including distributed tin (DT) wires consisting of separate modules of Nb filaments and Sn sources within a common diffusion barrier [14], [15], [18]; and wire development for 14+ T accelerator magnets continues towards a target J_c of 1500 A mm^{-2} (at 16 T and 4.2 K) defined for the proposed FCC-hh hadron collider [13]. DT wires have been developed by two manufacturers: Kiswire Advance Technology (KAT, South Korea) in collaboration with CERN, and JASTEC (Japan) in collaboration with CERN and the High Energy Accelerator Research Organization, KEK (Japan).

A comparative investigation has been performed into the effects of cabling and rolling on RRP, PIT and DT Nb₃Sn wires of several designs. The I_c, RRR and magnetothermal stability has been measured for virgin and rolled samples, and for strands extracted from cables, and assessed in relation to the corresponding deformation and wire design observed by electron microscopy and quantified by image analysis. For RRP and bundle-barrier PIT wire, a statistical analysis has also been performed over large quantities of wire procured, systematically characterized and cabled at CERN.

Based on this analysis, the susceptibilities of different wire designs to degradation on rolling and cabling are compared, the utility of rolling degradation as a predictor of cabling degradation is reviewed, and recommendations for future acceptance test procedures are made.

II. CONDUCTORS

A. Wire Designs

This study considers six designs of RRP wire from Bruker OST; DT wires from two suppliers, KAT and JASTEC; and bundle-barrier PIT (PIT-BB) from Bruker EAS.

The characteristics of the RRP wires are summarized in Table I, and the layouts are shown schematically in Fig. 1.

Further characteristics and cross-sections have been reported previously [15]. The 162/169 layouts at 1.0 mm (ERMC-1) and 1.1 mm (DEM-1.1) diameter were designed targeting high I_c, with a higher Sn stoichiometry and a low Cu/non-Cu ratio ∼0.9. DEM-1.1 in particular is used for the high field coil in graded designs, paired with the high-Cu DEM-0.7 wire for the low-field coil. All other wires have a Cu/non-Cu ratio ∼1.2 and reduced Sn stoichiometry.

The DT and PIT-BB wires all include a common external diffusion barrier and a layout of 192 filaments or Sn/Nb modules. Their characteristics are summarized in Table II. The PIT-BB wire is the only one here with nominally circular filaments (all other modules/sub-elements are nominally hexagonal). The KAT wire is the same design previously reported as 'trial 5' [15], with the distinguishing feature of an additional internal diffusion barrier.

Cross-section micrographs are presented in Fig. 2.

B. Cable Designs

The wire types listed above have been used for the production of Rutherford cables with the nominal characteristics tabulated
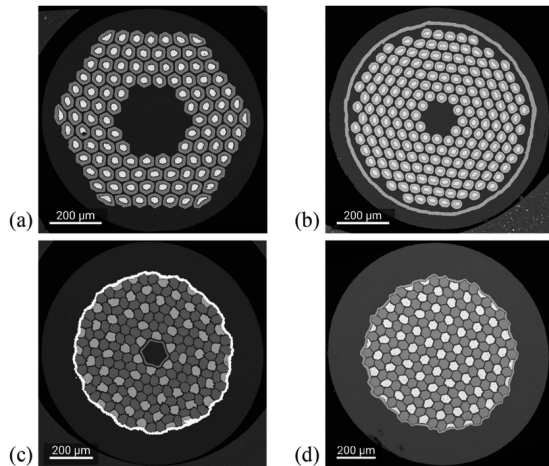
Fig. 2. Backscattered electron micrographs of the cross-sections of (a) RRP MQXF, (b) PIT-BB, (c) KAT DT, and (d) JASTEC DT wires in virgin condition.

TABLE III
CABLE DESIGNS

Property	MQXF	FalconD	R2D2 HF
RRP wire type for production use	MQXF (108/127)	ERMC-1 (162/169)	DEM-1.1 (162/169)
Wire types for trials/development	PIT-BB 192	KAT	JASTEC
Strands, number × diameter (mm)	40 × 0.85	40 × 1.0	21 × 1.1
Cable pitch (mm)	109	110–120	84
Keystone (°)	0.4	0.5	None
Core	Steel [a]	Steel [a]	None
Width (mm)	18.15	20.95	12.579
Mid-thickness (mm)	1.525	1.80	1.965

[a] Stainless steel 1.4404 (316L), 0.025 mm thick

Fig. 3. Example cross-section (optical micrograph) of a Rutherford cable produced with the FalconD design using KAT DT wire before heat treatment.

in Table III. The mid-thickness of these designs corresponds to ∼11% reduction in strand diameter at the center of the cable.

The cable designs are named according to the magnet application for which they were developed. At present only RRP wire is used for production of the magnets concerned (e.g., the MQXF cable design, produced using the 108/127 RRP wire type identified as 'MQXF' in Table I, is used for the HL-LHC quadrupole magnets), but the same cable designs have been used for trial cabling to assess the suitability of DT wires (see Fig. 3).

III. SAMPLES AND METHODS

I_c and RRR measurements, and electron microscopy, were performed on samples after heat treatment under vacuum. Samples for measurement of I_c (and quench current) were wound on Ti-Al-V barrels, reacted in a large tube furnace under vacuum, and measured on the same barrels; samples for measurement of RRR and for microscopy were reacted alongside the barrels.

Virgin/round wire samples are cut from the wire spool as received. Rolled samples are prepared by uniaxial rolling, and the rolling reduction is defined as the reduction in thickness relative to the original diameter. For routine wire acceptance tests presented here, a rolling reduction of 15% is used. In addition, for the RRP MQXF, PIT-BB, KAT and JASTEC wires, several adjacent samples from the same spool were rolled with reductions of 15%, 17.5%, 20% and 30%.

Extracted strands are strands removed from a cable after production for measurement. Cabling degradation (of I_c or RRR) is calculated relative to a representative virgin sample, which wherever possible originates from a position in the original wire spool adjacent to the extracted strand.

RRR values are defined as the ratio of the resistance at 293 K and 20 K. Transport I_c measurements were performed in applied magnetic fields of up to 15 T, and at temperatures of nominally 1.9 K (superfluid He-II) and 4.3 K (liquid helium). I_c is calculated using a 0.1 μV/cm criterion. Stability was evaluated from V-I measurements, which primarily test self-field stability [15]. Several measurements were performed at each magnetic field, for each of which the maximum current reached ($I_{\max}$) was recorded for a ramp rate of 12 A/s, corresponding to the quench current in case of premature quench. $I_{\max}$ and I_c are presented without adjustment for the sample self-field or measured temperature.

Scanning electron microscopy (SEM) was performed using a Zeiss Evo 10 microscope on metallographic samples mounted in transverse cross-section. Image analysis of backscattered electron micrographs was performed using cus-tom Python scripts and the scikit-image library for post-processing, segmentation and analysis.

IV. ROLLING DEFORMATION OF RRP AND PIT WIRES

A. RRP Wires

For a single spool of MQXF RRP wire, several samples were taken with rolling reductions of 0%, 15%, 17.5%, 20% and 30%. Selected electron micrographs of these unreacted samples are shown in Fig. 4. For 15% rolling reduction, the distortion primarily of sub-elements close to the shear planes at ±45° to the rolling direction is evident (Fig. 4(a)): the aspect ratio of sub-elements in these regions increases, with local thinning of the diffusion barrier and reduced separation from neighboring sub-elements. This distortion increased with further rolling (Fig. 4(b)), and for 30% rolling reduction (Fig. 4(c)), sub-element merging, shearing and barrier breakages occurs for multiple sub-elements.

Very similar observations were also made in reacted micrographs, except that areas increase (and separations decrease) due to the volumetric expansion on formation of Nb₃Sn from Nb. Local barrier thinning at 20% rolling reduction tends to result in complete local reaction of the barrier, for example.

This evolution of the sub-element geometry has been quantified by image analysis. Fig. 5 shows the evolution of the sub-element aspect ratio distribution with increasing rolling reduction. The mean and the variability of aspect ratios increases progressively with rolling reduction, and this increase
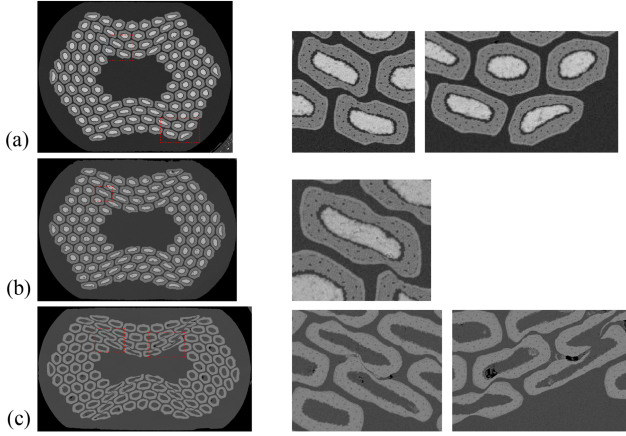
Fig. 4. Backscattered electron micrographs of the cross-sections of RRP MQXF wire (108/127) before heat treatment with rolling reductions of (a) 15%, (b) 20%, and (c) 30%: Images on the right are enlargements of the marked regions on the whole wire cross-sections.
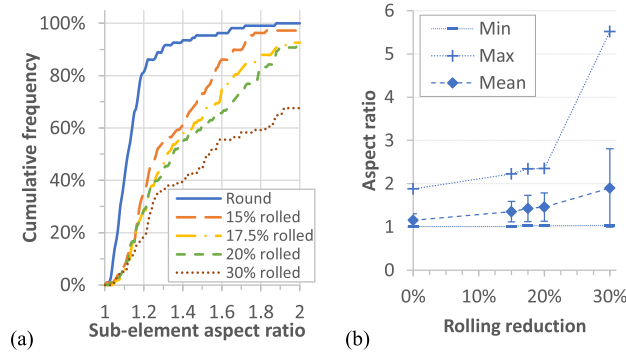

Fig. 5. Sub-element aspect ratios in RRP MQXF wire (108/127) before heat treatment for the round wire and for rolling reductions of 15%, 17.5%, 20%, and 30%: (a) Cumulative aspect ratio distributions and (b) Statistics of the aspect ratio distribution as a function of rolling reduction (error bars represent the standard deviation).

accelerates above 20% rolling reduction. Isolated cases of extremely high aspect ratio correspond to merged sub-elements.

A recent study of cable deformation selected an aspect ratio of 1.8 as a value of interest, noting that this value is exceeded by <5% of sub-elements near the cable center, but up to 30% of sub-elements for strands in the most distorted edge locations [9], [10]. Interpolating in the results of Fig. 5, these would correspond to rolling reductions of approximately 15% and 25%.

The images in Fig. 4 were selected to show a consistent orientation of the sub-element pack relative to the rolling direction, but it should be noted that all orientations will be present in a measurement sample (both for the rolling study and in cabling): the twist pitch of the wire sub-elements, and the transposition length of the cable, are both shorter than usual RRR and I_c sample lengths. Imperfect geometrical uniformity along the wire length may also mean that the threshold for sub-element damage on deformation may be met intermittently even for lower rolling reductions, and affect I_c and/or RRR, without necessarily being observable in any individual chosen cross-section.

The effect of these geometrical changes on I_c and RRR is shown in Fig. 6. RRR decreases continuously with increasing
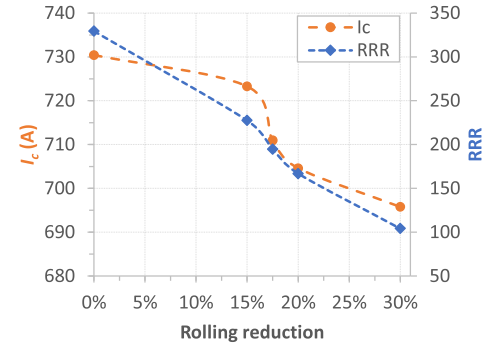

Fig. 6. Dependence of I_c (at 12 T and 4.2 K) and RRR on rolling reduction for RRP MQXF wire (108/127). Markers represent the mean of measured values; dashed lines are a guide to the eye only.
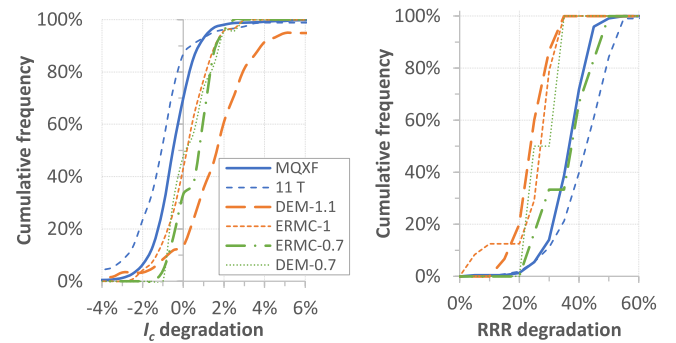

Fig. 7. Cumulative distributions of the degradation of I_c and RRR for a rolling reduction of 15% for each RRP wire design. Wire designs are color coded by restack: Blue – 108/127, orange – 162/169, green – A/91.

rolling reduction; whilst I_c shows very little reduction for 15% rolling reduction, but decreases particularly steeply in the 15–20% rolling reduction range. These trends are not unexpected. The resistivity is very sensitive to even small amounts of Sn contamination, and local reductions in the diffusion distance between the Sn core and the interface between the matrix and diffusion barrier are evident in Fig. 4(a); whilst a corresponding small Sn loss would not be expected to significantly reduce the volume of Nb_3Sn formed (and under-reaction was not observed in reacted micrographs). These values of RRR remain sufficiently high for magnet applications: the HL-LHC MQXF cable specification [11] requires a RRR of 100 in extracted strands, and for the present sample this was retained even for 30% rolling.

The strong dependence of I_c on rolling reduction for values close to the 15% conventionally used for acceptance tests, however, is undesirable: small errors in rolling reduction due to poor equipment tolerances or roll wear could increase the variability in measured values.

For a rolling reduction of 15%, data from acceptance tests are available for a significant number of spools of RRP wire with different designs. The cumulative distributions of I_c and RRR degradation are shown in Fig. 7. For the MQXF wire analyzed above, the mean I_c degradation is negative (−0.6%): this is not necessarily a statistical artefact, an increase in I_c on rolling may arise from (e.g.,) reduced diffusion distances, and this has been observed previously in other wire types. It is also
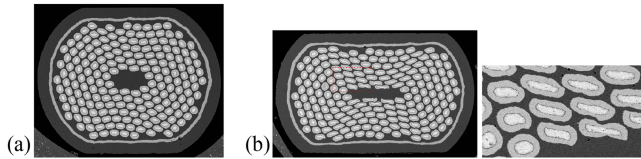
Fig. 8. Backscattered electron micrographs of the cross-sections of PIT-BB wire before heat treatment with rolling reductions of (a) 15% and (b) 30%: The image on the right is an enlargement of the marked region.
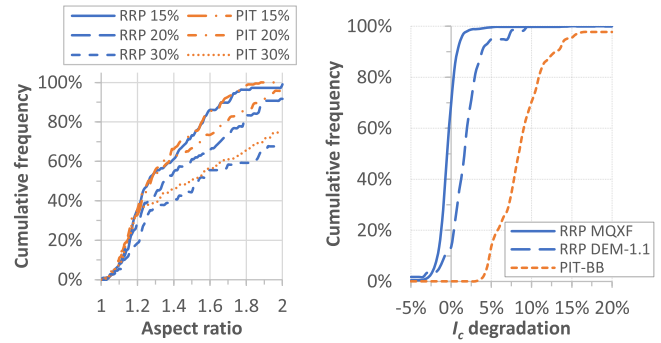

Fig. 9. Cumulative distributions of (a) aspect ratios of RRP sub-elements and PIT filaments for the RRP MQXF wire (108/127) and PIT-BB wires before heat treatment, for rolling reductions of 15%, 20%, and 30% and (b) the I_c degradation of PIT-BB, RRP MQXF (108/127) and DEM-1.1 (162/169) wires for a rolling reduction of 15%.

striking that the 162/169 wires (and especially DEM-1.1) show significantly higher I_c degradation, but lower RRR degradation, than the 108/127 wires.

For HL-LHC RRP cables, there is an acceptance criterion of 5% I_c degradation for extracted strands: for 15% rolling, this is met for substantially all MQXF wires, but failed for 5% of DEM-1.1 wires. The difference in behavior may not arise solely from the wire restack – there are also differences in Sn stoichiometry and Cu/non-Cu ratio, the balance of I_c and RRR can be adjusted by heat treatment optimization. It should also be noted that this is consistent with previous reports of higher cabling degradation for the DEM-1.1 wire [15], but not with earlier studies of 169-stack wires, which found negligible I_c degradation for 15% rolling [7]. Understanding the reasons for the difference will require further study, and contributions from wire defects are not excluded. This observation demonstrates the need for testing and optimization even for the established and robust RRP wire type, and highlights an added value of rolling tests: without these data identifying a need for optimization at strand or heat treatment level, one may have concluded that excessive cabling degradation required a change of cable design.

B. Comparison of PIT-BB and RRP Wires

The structure of PIT wires differs significantly from RRP. PIT filaments are approximately circular in cross-section, and the region in which Nb₃Sn forms is originally a powder-filled continuous Nb-Ta tube rather than a distribution of fine Nb filaments in Cu, which might be expected to affect the detailed deformation behavior. Indeed the typical geometrical imperfections in virgin round wire differ between RRP and PIT: whilst the latter may have a broader aspect ratio distribution overall, RRP wires have more highly distorted sub-elements in the corner positions of the outer ring [8], and PIT wires are more susceptible to offsets in the centers of the powder cores and the tubes [19]. Some similar features arise on rolling (Fig. 8) – aspect ratios increase, especially at and between the ±45° shear axes, and at 30% rolling reduction local barrier thinning occurs in a significant number of filaments–but complete merging or shearing of filaments is not observed.

The evolution of the aspect ratio distribution is actually remarkably similar for RRP and PIT-BB wires, as also found previously for PIT wires without a bundle barrier [4], [8], but the performance impact of these geometrical changes differs dramatically (Fig. 9).

The external barrier in PIT-BB robustly protects the outer copper sampled in a RRR measurement, so apparent RRR
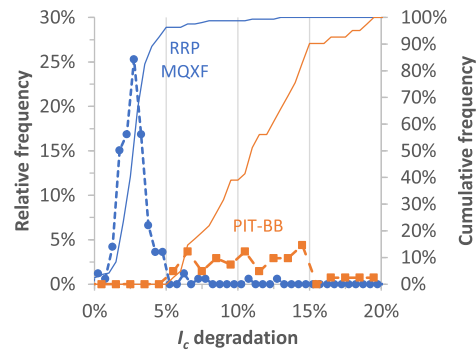

Fig. 10. I_c degradation distribution (relative on left axis, dashed lines; cumulative on right axis, thin solid lines) for extracted strands of the RRP MQXF (108/127) and PIT-BB wires from cables with the MQXF design.

degradation is typically very low (mean 2%). The I_c degradation for 15% rolling reduction is, however, both more variable and higher on average (8.8%) than comparable RRP wire designs (e.g., −0.6% for MQXF).

This partly reflects the different processes of Nb₃Sn formation in the two cases. In RRP, outward Sn diffusion (and inward Cu diffusion) occur through the Nb region throughout the heat treatment, as the Nb is divided into small filaments separated by Cu channels. Sn loss in the final heat treatment plateau is from the adjacent relatively Sn-poor Cu-Sn region, and has little impact on the volume of Nb₃Sn formed. By contrast, in PIT, Sn loss through a breached or locally thinned barrier is from the Sn-rich core, and as the kinetics of Nb₃Sn slow due to diffusion through the growing Nb₃Sn layer during the final heat treatment plateau, reaction of a filament effectively stops as soon as tin loss begins locally.

C. Comparison of Rolling and Cabling Degradation

For the HL-LHC Project, series production of MQXF cables has been performed using RRP wire, and during the development stage a significant number were also produced with PIT-BB. The I_c degradation distribution is presented for both types in Fig. 10. The mean I_c degradation on cabling is significantly higher than the mean degradation for 15% rolling reduction in both cases:

2.8% for RRP MQXF, 11% for PIT-BB. For RRP, the mean I_c degradation on cabling is comparable to the I_c degradation for 17.5% rolling. For PIT, the degradation distributions are also much broader than for RRP both for rolling and cabling.

By contrast, the mean RRR degradation on cabling of RRP MQXF wire is 16.9%, approximately half that of 15% rolled samples. RRR measurements are performed with a voltage tap spacing of 51.3 mm or 71.5 mm typically including 1–2 cable edges, and effectively provide a weighted average of the behavior at and away from the edges. Positions near the center of the cable (corresponding to the majority of each strand) have a thickness reduction of <15% (typically ~11%), so it is not surprising that the average RRR is less degraded than for a sample uniformly rolled with 15% reduction.

For two extracted strand samples of RRP MQXF cable, the RRR was measured locally at each cable edge, near the cable center and over the full length. For the localized measurements, the voltage tap spacing was ~5 mm. Relative to the full-length value, the RRR was found to be on average 9% and 27% lower at the thick and thin edges respectively, and 9% higher at the center. For a conservative evaluation of coil behavior, especially considering the differences in behavior between wire types, it would be desirable to systematically test these local minimum RRR values in extracted strands, and work is in progress to develop a suitable sample holder.

For a conservative evaluation of strand I_c, consideration should also be given to testing at an increased rolling reduction of at least 17.5%, or using samples with a non-uniaxial deformation more representative of cabling deformation at the thin edge (e.g., rolling of strands in a triplet configuration [10]).

V. ROLLING AND CABLING DEFORMATION OF DT WIRES

Previous analysis of the rolling behavior of DT wires noted that there is a tendency for softer Sn regions to deform and merge, while comparatively hard Nb modules (i.e., assemblies of Nb filaments in Cu, without an external diffusion barrier) remain largely intact and are displaced relative to each other. For the present 1.1 mm diameter JASTEC wire, a similar behavior is observed, as shown in Fig. 11: shearing of just the outermost Nb filaments of a module becomes apparent at 20% rolling reduction.

There is significant variability between cross-sections, perhaps according to the orientation of the restack relative to the rolling direction. Visually, one may consider these in two categories: cases like Fig. 11(b) above, with Sn merging near the wire center, and cases like Fig. 11(a) and (c) above, with visible ±45° bands. Nevertheless, the behavior of the Nb modules is similar in both cases.

Fig. 12 shows maps of the Nb module aspect ratio for examples with 15%, 20% and 30% rolling reduction: the majority of modules retain an aspect ratio ~1.2 even for a 30% rolling reduction, in contrast to the broad distribution of large aspect ratios for RRP in Fig. 5. When clear ±45° shear planes are evident in the wire micrograph, there is no corresponding pattern in the color map: this deformation is accommodated by the separation of the Nb modules rather than distortion.
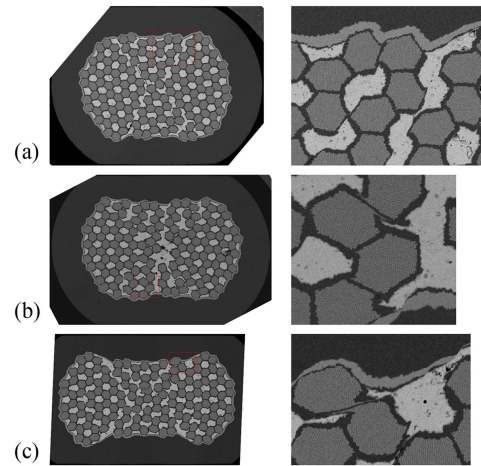

Fig. 11. Backscattered electron micrographs of the cross-sections of JASTEC DT wire before heat treatment with rolling reductions of (a) 15%, (b) 20%, and (c) 30%: Images on the right are enlargements of the marked regions on the whole wire cross-sections.
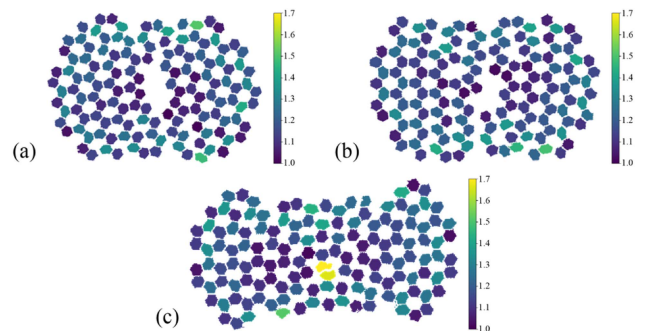

Fig. 12. Color maps showing the aspect ratio of Nb modules in unreacted JASTEC DT wire samples with rolling reductions of (a) 15%, (b) 20%, and (c) 30%.
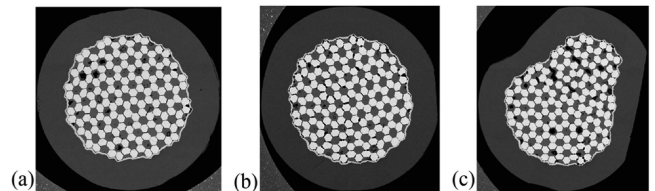

Fig. 13. Backscattered electron micrographs of JASTEC DT wire after heat treatment: (a) Virgin wire, (b) extracted strand near the cable center, and (c) extracted strand near the cable edge.

After reaction, this relative movement of Nb modules can result in contact (or near contact) between adjacent Nb$_3$Sn regions (Fig. 13). This increase in effective filament diameter (d_{eff}) is expected to increase magnetization and have an adverse effect on magnetothermal stability. Excluding these large effective filaments from the image analysis, the remaining modules show a very similar aspect ratio distribution for virgin wire and for extracted strands both near the cable center and edge, with a mean below 1.2 (Fig. 14).

For KAT wires, observations of module geometry are broadly similar. The internal diffusion barrier constrains Sn flow during rolling/cabling, preventing cases like Fig. 11(b) observed for JASTEC above. The barrier becomes significantly distorted for
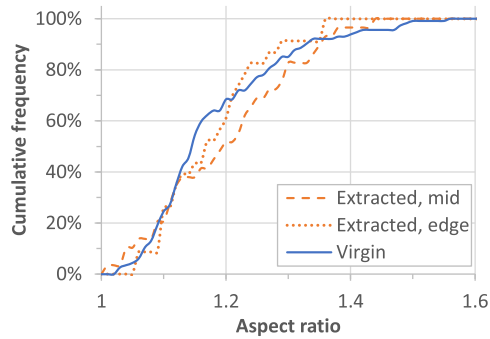
Fig. 14. Distribution of the aspect ratio of Nb$_3$Sn regions in reacted JASTEC DT wire samples, excluding regions of two or more Nb modules in contact.
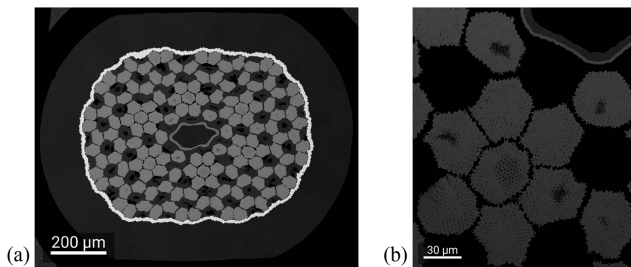

Fig. 15. Backscattered electron micrographs of (a) 20% rolled KAT DT wire after heat treatment and (b) enlargement of a region near the strand center.
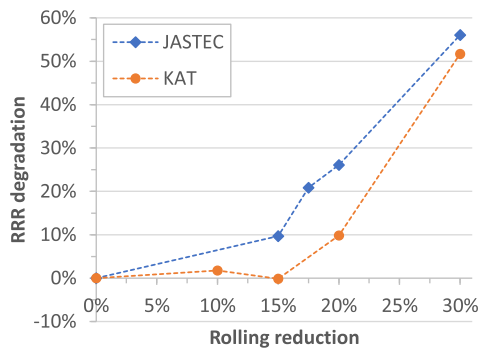

Fig. 16. RRR degradation on rolling of JASTEC and KAT (see [12]) DT wires.

20% rolling and above (Fig. 15), but breaches would have little direct performance impact due to the relatively small area of Cu enclosed. It is also evident that a reaction layer grows on the barrier (Fig. 15(b)), potentially contributing to increased magnetization and/or Sn depletion. Some clusters of 7 modules are found to be in close proximity after reaction (Fig. 15(b)), and intermittent contact could contribute to increased d_{eff} and reduced stability. Some unreacted Nb remains in the centers of Nb modules (darker contrast in Fig. 15), and curiously these are not always in modules furthest from the original Sn sources: this suggests some potential to increase I_c, and requires further study.

The external diffusion barriers are effective in preserving high RRR. The RRR degradation is a little higher for JASTEC than KAT (Fig. 16), with the onset of measurable degradation at a lower rolling reduction (15%); but in both cases, the degradation for 15% rolling reduction is <10%, significantly lower than
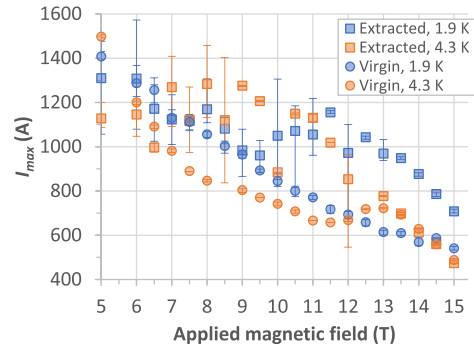

Fig. 17. Imax (in most cases equal to the quench current) as a function of applied magnetic field for extracted and virgin strands of JASTEC wire from a cable with the R2D2 HF design, at nominal temperatures of 1.9 K and 4.3 K. Markers show the average $I_{\max}$ for each field; error bars indicate the minimum and maximum measured.

the mean for RRP wires (Fig. 7). As previously reported, mean extracted strand RRR was comparable to a rolling reduction of 20% for the KAT wire [15].

Stability limitations were experienced in the I_c measurement of both wire types, so there is not sufficient data to robustly quantify I_c degradation on rolling or cabling. The limited data available so far [15] suggest I_c degradation is low, as might be expected from the relative integrity of the Nb modules and the low Sn loss suggested by the analysis above.

V-I stability measurements of the virgin JASTEC DT wire, and a strand of JASTEC DT wire extracted from a cable produced with the R2D2 HF layout, are presented in Fig. 17. Unusually, the quench currents of the virgin wire were much lower than those of the extracted strand, but the latter showed much greater variability between quench currents: tests of additional samples will be required to validate the true behavior. Very few measurements allowed a reliable I_c value at the usual criterion to be determined, so an $I_c(B)$ fit is not attempted here; the mean $I_{\max}$ value for virgin wire at 4.2 K and 15 T would correspond to a non-Cu J of 1068 A/mm^2.

It is clear that the performance is limited by magnetothermal instability, but one promising indication is that quench currents for the extracted strand at 1.9 K exceed those at 4.3 K for applied magnetic fields down to ∼11 T. For comparison, the previously reported quench currents of rolled KAT samples at 1.9 K decreased below those at 4.3 K for an applied field as high as 14.5 T [15]. There are tentative indications in the high-field region that quenches are occurring very close to the true critical current value, even at 1.9 K. For marginal values, it is possible that heat treatment optimization may improve stability behavior sufficiently to allow consistent I_c characterization [15], but the observations of closely-spaced reacted Nb$_3$Sn regions and local incomplete reaction suggest that further optimization of the wire designs may be needed.

VI. SUMMARY

Analysis of the rolling and cabling deformation behavior of RRP, PIT and DT wires has identified consistent trends for each wire type, but also significant differences between specific designs.

In RRP and PIT wires, deformation is concentrated along clear planes, and primarily accommodated by shearing of the sub-elements/filaments. For PIT-BB wires, the I_c degradation on rolling or cabling is significantly higher and more variable than for all RRP designs tested. This characteristic cannot be attributed to the aspect ratio distribution of the filaments alone, which evolves comparably on deformation to RRP wires. All RRP wires tested show a reasonably narrow distribution of I_c and RRR degradation for a 15% rolling reduction, with the majority of samples not exceeding 5% I_c degradation, but the degradation is significantly higher for (e.g.,) DEM-1.1 (162/169 at 1.1 mm) than MQXF (108/127 at 0.85 mm) wires. Without rolling data identifying a need for strand optimization, one may have concluded that excessive cabling degradation required a change of cable design. It is not possible to fully distinguish the effects of layout, Sn stoichiometry, Cu/non-Cu and heat treatment: but this emphasizes the need to carefully assess each wire design, and optimize its heat treatment as well as the cabling parameters.

In DT wires, strain is primarily accommodated by distortion of Sn modules, with relative displacement of Nb modules. RRR degradation is well controlled for both KAT and JASTEC wires, and there is little evidence of I_c degradation, but further wire development is needed to enhance magnetothermal stability. The displacement of Nb modules during rolling or cabling is one characteristic potentially increasing d_{eff}.

Uniaxial rolling is a useful approximation of wire deformation behavior for initial wire design qualification and acceptance tests, but a 15% rolling reduction is not a conservative value for the evaluation of I_c degradation (17.5% appears more representative of the RRP cables reported here), and nor is it a stable choice, as rapid change in I_c or RRR often arises in the 15–20% rolling reduction range. The use of a higher rolling reduction should therefore be considered. A single value of rolling reduction cannot be expected to be representative of all wires and cables: the criterion should be reviewed for future designs. The use of alternative mechanical approaches (e.g., [10]) to better approximate cabling deformation should also be investigated.

Similarly, the RRR degradation of 15% rolled samples is higher than that of extracted strands for RRP wires, but lower than extracted strands for KAT DT samples; and the RRR measured locally at a cable edge has been found to differ by $\sim$30% from the overall value for MQXF RRP samples. For cable qualification, and benchmarking of wire acceptance test procedures, it is therefore proposed that RRR should be routinely measured on unstraightened samples both locally at the cable edges and near the cable center.

REFERENCES

[1] E. Barzi, D. Turrioni, and A. V. Zlobin, "Progress in Nb$_3$Sn RRP strand studies and Rutherford cable development at FNAL," *IEEE Trans. Appl. Supercond.*, vol. 24, no. 3, Jun. 2014, Art. no. 6000808.

[2] D. Turrioni et al., "Effects of Rutherford cable parameters on Nb$_3$Sn extracted strand deformation and performance," *IEEE Trans. Appl. Supercond.*, vol. 18, no. 2, pp. 1114–1117, Jun. 2008.

[3] M. D. Sumption et al., "Effect of cable edge deformation on RRR and magnetization of strands extracted from Nb$_3$Sn Rutherford-type cables," *IEEE Trans. Appl. Supercond.*, vol. 19, no. 3, pp. 2481–2485, Jun. 2009.

[4] D. Turrioni et al., "Study of effects of deformation in Nb$_3$Sn multifilamentary strands," *IEEE Trans. Appl. Supercond.*, vol. 17, no. 2, pp. 2710–2713, Jun. 2007.

[5] A. A. Polyanskii et al., "Evidence for highly localized damage in internal tin and powder-in-tube Nb$_3$Sn strands rolled before reaction obtained from coupled magneto-optical imaging and confocal laser scanning microscopy," *Supercond. Sci. Technol.*, vol. 22, 2009, Art. no. 095008.

[6] E. Z. Barzi, M. Bossert, and G. Gallo, "A model to study plastic deformation in RRP Nb$_3$Sn wires," *IEEE Trans. Appl. Supercond.*, vol. 21, no. 3, pp. 2588–2592, Jun. 2011.

[7] E. Barzi et al., "Studies of Nb$_3$Sn strands based on the restacked-rod process for high field accelerator magnets," *IEEE Trans. Appl. Supercond.*, vol. 22, no. 3, Jun. 2012, Art. no. 6001405.

[8] M. Brown, C. Tarantini, W. Starch, W. Oates, P. J. Lee, and D. C. Larbalestier, "Correlation of filament distortion and RRR degradation in drawn and rolled PIT and RRP Nb$_3$Sn wires," *Supercond. Sci. Technol.*, vol. 29, no. 8, 2016, Art. no. 084008.

[9] A. Baskys et al., "RRP Nb$_3$Sn subelement shear dependence on hexagonal subelement stack orientation and the strand's position within a Rutherford cable," *IEEE Trans. Appl. Supercond.*, vol. 33, no. 5, Aug. 2023, Art. no. 4801605.

[10] A. Baskys et al., "RRP Nb$_3$Sn sub-element shear dependence on sub-element stack orientation and the strand's position within a Rutherford cable," presented at the Appl. Supercond. Conf. 2022, Honolulu, HI, USA, Oct. 27, 2022.

[11] L. D. Cooley, A. K. Ghosh, D. R. Dietderich, and I. Pong, "Conductor specification and validation for high-luminosity LHC quadrupole magnets," *IEEE Trans. Appl. Supercond.*, vol. 27, no. 4, Jun. 2017, Art. no. 6000505.

[12] B. Bordini et al., "The bundle-barrier PIT wire developed for the HiLumi LHC project," *IEEE Trans. Appl. Supercond.*, vol. 27, no. 4, Jun. 2017, Art. no. 6000706.

[13] A. Ballarino and L. Bottura, "Targets for R&D on Nb$_3$Sn conductor for high energy physics," *IEEE Trans. Appl. Supercond.*, vol. 25, no. 3, Jun. 2015, Art. no. 6000906.

[14] S. C. Hopkins, A. Baskys, B. Bordini, J. Fleiter, and A. Ballarino, "Design, performance and cabling analysis of Nb$_3$Sn wires for the FCC study," *J. Phys.: Conf. Ser.*, vol. 1559, 2020, Art. no. 012026.

[15] S. C. Hopkins, B. Medina-Clavijo, C. Barth, J. Fleiter, and A. Ballarino, "Design optimization, cabling and stability of large-diameter high J_c Nb$_3$Sn wires," *IEEE Trans. Appl. Supercond.*, vol. 33, no. 5, Aug. 2023, Art. no. 6000609.

[16] A. Pampaloni et al., "Mechanical design of FalconD, a Nb$_3$Sn Cosθ short model dipole for the FCC," *IEEE Trans. Appl. Supercond.*, vol. 32, no. 6, Sep. 2022, Art. no. 4000605.

[17] V. Calvelli et al., "R2D2, the CEA graded Nb$_3$Sn research racetrack dipole demonstrator magnet," *IEEE Trans. Appl. Supercond.*, vol. 31, no. 5, Aug. 2021, Art. no. 4002706.

[18] S. Kawashima et al., "Development of a high current density distributed tin method Nb$_3$Sn wire," *IEEE Trans. Appl. Supercond.*, vol. 30, no. 1, Jan. 2020, Art. no. 6000105.

[19] C. B. Segal, "Performance limits of powder in tube processed Nb$_3$Sn superconducting wires," Ph.D. dissertation, Dept. Mech. Eng., Florida State Univ., Tallahassee, FL, USA, 2018. [Online]. Available: http://purl.flvc.org/fsu/fd/2018_Sp_Segal_fsu_0071E_14456